

RESEARCH

Open Access



Mechanical properties of white clay used as wall painting substrate material: measurement of strength and modulus of elasticity of simulated substrate material of wall paintings *Hiten* at *Kondo*, the main hall at Horyu-ji Temple

Kazuki Ishikawa^{1*}, Daisuke Ogura¹, Chiemi Iba¹, Nobumitsu Takatori¹ and Soichiro Wakiya²

Abstract

Preserving cultural artifacts while minimizing the energy consumption and costs associated with environmental control is crucial. This often requires predicting artifacts degradation caused by temperature and humidity. Here, mechanical damage can be predicted by comparing stress and damage criteria. Although the constitutive coefficients and damage criteria of various materials have been extensively studied, the mechanical properties of white clay remain unknown. This material is a crucial component of various artifacts including some important cultural artifacts and national treasures of Japan. Thus, this study aims to identify the strength and elastic properties of simulated white clay mimicking the substrate of the wall paintings *Hiten* at *Kondo*, the main hall at Horyu-ji Temple. Following existing literature, we created the simulated white clay by combining clay, paper fiber, and rice glue. We fabricated 36 distinct specimen patterns by varying the equilibrium humidity and material mixing ratios. We measured the tensile strength using splitting tensile tests and, compressive strength, Young's modulus, and Poisson's ratio using compressive tests. The tensile strength, compressive strength, Young's modulus, and Poisson's ratio ranged from 0.0785–1.17 (MPa), 0.358–3.67 (MPa), 0.0394–0.274 (GPa), and 0.10–0.44(-), respectively, with variations depending on the equilibrium humidity and ratio of material mixing. We also formulated the results as functions that depend on the equilibrium humidity and material mixing ratios. These findings can be used to predict stress and damage to targeted wall paintings and to inform the preservation and restoration of cultural artifacts containing white clay.

Keywords Humidity, Mud wall, White clay, Splitting tensile test, Tensile strength, Compressive test, Young's modulus, Poisson's ratio, Compressive strength

*Correspondence:

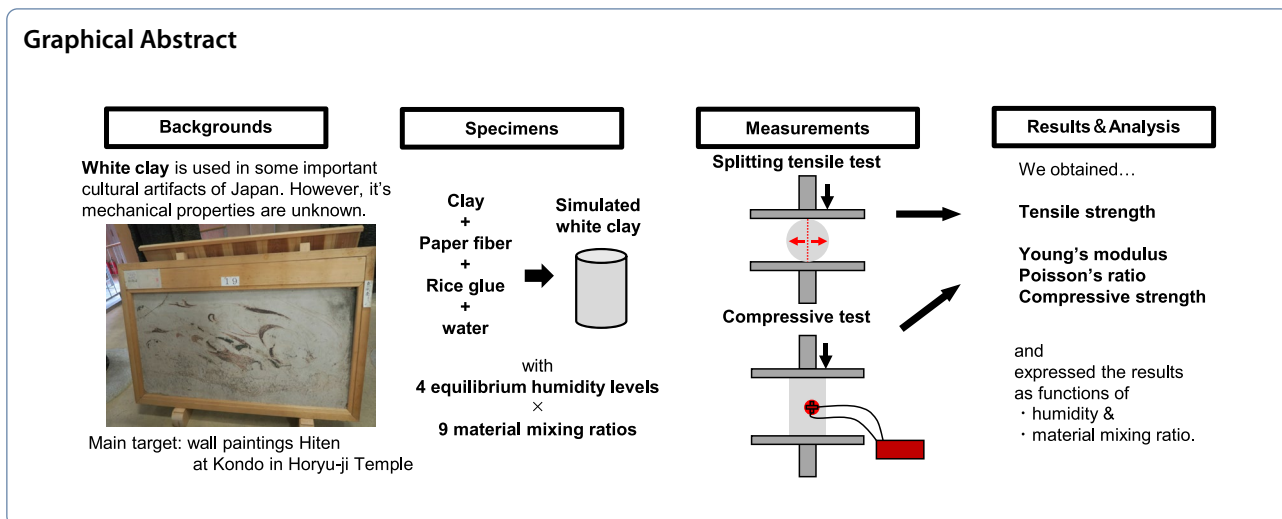
Kazuki Ishikawa

ishikawa.kazuki.75w@st.kyoto-u.ac.jp

Full list of author information is available at the end of the article



© The Author(s) 2023. **Open Access** This article is licensed under a Creative Commons Attribution 4.0 International License, which permits use, sharing, adaptation, distribution and reproduction in any medium or format, as long as you give appropriate credit to the original author(s) and the source, provide a link to the Creative Commons licence, and indicate if changes were made. The images or other third party material in this article are included in the article's Creative Commons licence, unless indicated otherwise in a credit line to the material. If material is not included in the article's Creative Commons licence and your intended use is not permitted by statutory regulation or exceeds the permitted use, you will need to obtain permission directly from the copyright holder. To view a copy of this licence, visit <http://creativecommons.org/licenses/by/4.0/>. The Creative Commons Public Domain Dedication waiver (<http://creativecommons.org/publicdomain/zero/1.0/>) applies to the data made available in this article, unless otherwise stated in a credit line to the data.



Introduction

Background

Cultural artifacts, such as paintings and sculptures stored in temples, shrines, and museums, can be damaged and lose value due to exposure to unfavorable temperatures and humidity. Long-term exposure to high temperatures and humidity can accelerate chemical and biological deterioration. Additionally, cultural artifacts composed of hygroscopic materials can deform owing to changes in temperature or humidity. Here, sudden changes, including those caused by turning air conditioning on and off, can cause mechanical damage such as irreversible deformations, cracks, and delamination [1]. Although environmental controls in storage facilities are crucial, it is also important to consider energy and cost reductions. To prevent the deterioration of cultural artifacts while meeting these requirements, acceptable fluctuations and rates of change in temperature and humidity must be determined over time. Therefore, it is necessary to predict the initiation and progression of degradation resulting from unstable environmental conditions.

This study focuses on mechanical damage, a form of deterioration in stored cultural artifacts composed of hygroscopic materials. Such damage arises when the temperature and moisture content vary within a material or when materials with different expansion and contraction rates are bonded, leading to stress that exceeds the strength of the material owing to constrained deformation. In paintings, materials with different moisture/thermal expansion coefficients are attached in layers and constrained to each other. Furthermore, when the environmental humidity/temperature changes, the material reaches moisture/heat equilibrium from near the surface, resulting in a moisture content/temperature distribution in the thickness direction. For example, when

the environment dries out, the surface layer dries first and tries to shrink. However, the inner side, where the moisture content has not changed, is not deformed, and subsequently, the tensile force is loaded on the surface layer. Extant studies have described a similar mechanism of occurring stress [2, 3]. Furthermore, when the materials of the surface layer and the inner side are different, even if the inner side reaches equilibrium, deformation is constrained according to the difference in the moisture expansion coefficients, and stress occurs.

Damage prediction needs to compare stress or strain to damage criteria. The stress and strain field corresponding to moisture content/temperature distribution can be calculated from the constitutive relations factoring constitutive coefficients such as Young's modulus and Poisson's ratio, as well as the moisture/thermal expansion coefficient. The moisture content/temperature distribution within a material can be predicted by heat and moisture simultaneous transfer models [4] when the environmental humidity/temperature changes. By utilizing such a prediction model, we can determine the allowable environmental humidity/temperature fluctuation from the viewpoint of damage prevention. To create the prediction model, we must understand the constitutive coefficients of the materials in question, the moisture/thermal expansion coefficients, and damage criteria such as strength.

Existing literature and research motivation

The mechanical properties of materials used in various cultural artifacts have been studied extensively, and predictions of deformation and damage have been made to conserve and utilize these artifacts safely. Mecklenburg [5, 6] investigated the strength; strain at failure; yield strain; elastic modulus of materials of panel paintings and

canvas paintings such as oiled paint, gessoes, hide glue, some species of wood, and linen; as well as equilibrium RH/temperature-strain relations. Furthermore, by comparing predicted stress and strength [5] or humidity/temperature-induced strain and critical strain leading to damage [6–8], Mecklenburg indicated the acceptable humidity and temperature fluctuation to conserve cultural artifacts safely. Many subsequent studies have followed his work.

Several studies have reported the coefficients of elastic constitutive laws. The relationship between the moisture content and mechanical state is typically defined as a moisture expansion coefficient, which quantifies strain according to moisture content or equilibrium RH and is integrated into the constitutive law. For example, the modulus of elasticity and moisture-related strain of poplar [9] and lime wood [2, 10] used in canvas paintings, panel paintings, and decorated wooden objects have been examined. Studies have also reported the modulus of elasticity [5, 10–14], Poisson's ratio [11, 12, 14], and moisture coefficients of dimensional change [5, 6, 11] for materials used in paintings, such as canvas, gesso, and oil paint. Furthermore, some researchers have considered the humidity dependence of these parameters [9, 11, 13]. The coefficients for the viscoelastic constitutive model were identified for the glues used in canvas consolidation, including the storage modulus [15, 16] and loss modulus [15].

Yield stress, strength, and degree of strain have often been examined as damage criteria. For cottonwood and white oak, the strength and yield strain at a range of RH have been examined [6]. For poplar wood, the strength and stress at the limit of proportionality have been measured [9]; for lime wood, stresses and strains at yield and failure have been investigated, as well as their humidity dependency [2]. The strength, yield stress and strains at break have been documented for oil paint [5, 6, 14] and animal glue [15]. Recently, there have been many applications of fracture mechanics as a model for predicting the evolution of existing flaws [3, 13, 17–21]. Some studies have reported the fracture path and toughness of oak wood of various ages [22] and the critical energy release rate of gesso [13]. Lacquer exported from East Asia, including Japan, sometimes had a foundation layer of clay mixed with a protein binder, in which delamination tends to occur [23]. Thus, the fracture energy of a mixture of hide glue and Japanese clay powder has been measured [24].

Additionally, the mechanical properties of various materials used in cultural artifacts have been examined for stress, deformation, and damage prediction, with some studies also revealing their humidity dependence. However, the scope of these investigations has

been limited primarily to canvas paintings and wooden objects such as panel paintings, cabinets, and statues. Some research has also been conducted on wool and silk in historic textiles [25] and Roman mortar used in historic buildings [26]. This indicates a significant gap in the understanding of the mechanical properties of many other materials used in cultural artifacts. Addressing this paucity is crucial in predicting the deterioration of such cultural artifacts.

One such material is white clay. White clay was extensively utilized in Japan between the seventh and fourteenth centuries as a substrate or pigment for wall paintings and a primary material for Buddhist statues [27]. Some studies have reported that historical wall paintings in China, Thailand, and Nepal have similar fine clay substrates [28–30], while others posit that white clay is a characteristic material in Japanese cultural properties [27]. Some cultural artifacts containing white clay still survive until today, such as the wall paintings at the main hall, *Kondo*, in the Horyu-ji Temple, clay sculptures at the Pagoda in the same temple, and wall paintings in the Toratsuka ancient burial tomb. Some of these artifacts are designated as important cultural properties or national treasures of Japan, highlighting the importance of this material. However, to the best of our knowledge, their mechanical properties have not been investigated. In the conservation and exhibition project of the wall paintings at the main hall in Horyu-ji Temple, where some authors are involved, it is crucial to predict the potential mechanical damage to wall paintings to develop suitable environmental control methods. Therefore, understanding the mechanical properties of the materials used in these wall paintings, particularly white clay, is important.

Research purpose

This study aims to identify the strength and elastic coefficients of white clay simulating the substrate material of wall paintings *Hiten* in the main hall of Horyu-ji Temple. Our findings can be utilized to construct a deformation and damage prediction model for wall paintings. White clay is produced by mixing clay with water, followed by drying and hardening. Since the macroscopic structure of white clay relies on the bonding of clay particles by the meniscus, its mechanical properties are expected to exhibit significant variations depending on the moisture state. Our research involved the preparation of specimens at different equilibrium humidity levels. We conducted tensile splitting test to measure the tensile strength and compressive test to identify Young's modulus, Poisson's ratio, and compressive strength. Additionally, the results were approximated as humidity-dependent functions,

which served as crucial inputs for the damage prediction model.

Main applicable objects

The wall paintings *Hiten*

Horyu-ji, a UNESCO World Heritage site, is known for housing the Saiin Temple complex, including the main hall, which are considered the oldest surviving wooden buildings in the world. Although the exact construction date was not recorded, scholars propose the main hall was built between the late 7th and early eighth century [31]. The first-floor walls of the main hall originally boasted 12 large wall paintings, whereas the upper walls featured 20 wall paintings depicting *Hiten*, symbolizing flying angels. The exact age of the wall paintings remains unclear [21]; however, it is believed that the building construction and creation of the wall painting were contemporaneous [27, 32]. During the extensive repair work of the Horyu-ji buildings in 1934, the main hall caught alight, significantly damaging the 12 wall paintings on the first-floor walls. However, the 20 *Hiten* wall paintings did not burn because they had been removed from the building frame along with their substrate walls for repair.

The *Hiten* wall paintings (Fig. 1) are classified as important cultural properties of Japan. One is exhibited in the Great Treasure Gallery (*Daihozoin*) of Horyu-ji, while the remaining 19 are stored in the storehouse alongside the burned and heavily damaged structure of the main hall and the large 12 wall paintings. Due to their value, these artifacts are typically stored under strict security measures and are not accessible to the public. However, recent attempts have been made to display them for a limited period. In our study, we observed the current state of the stored *Hiten* wall paintings in the storehouse of the main hall. Notably,



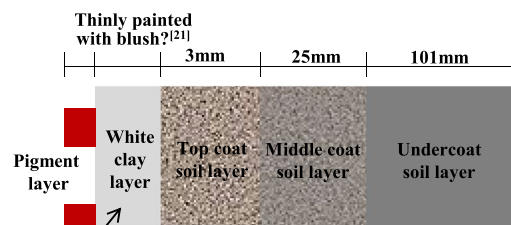
Fig. 1 One of the *Hiten* wall paintings in the main hall of Horyu-ji Temple

over half of the 19 paintings had visible surface cracks, and some displayed signs of delamination, particularly in the lower sections.

Material composition of the wall paintings

Determining the detailed material composition of cultural artifacts through nondestructive investigations is challenging, and the specific material composition of the *Hiten* wall paintings has not been fully elucidated. However, based on the available reports and previous studies, we made some assumptions about the material composition of the *Hiten* wall paintings, as depicted in Fig. 2.

According to a survey conducted in 1920 [33] and an analysis conducted following the repairs after the fire [31], in conjunction with existing literature [34–36], the wall paintings are presented on mud walls consisting of multiple layers. While materials in mud walls are typically plastered with a trowel, the white clay layer appears to have been thinly painted with a brush [31, 34]. Previous research [35] indicated that the chemical composition of the clay is similar to that of Amakusa pottery clay. This is a white, microscopic clay particle used in ceramic art and sourced from the Amakusa region in Japan. The materials used in the mud walls, including white clay, were naturally dried pastes made by mixing clay-containing soil with water, along with a fibrous material called *susa* and an adhesive called *nori*. In the traditional method of plastering mud walls, *susa* and *nori* are added to the mud paste. *Susa* is believed to enhance the resistance to tensile forces, whereas *nori* is believed to improve workability by increasing the elongation of the paste. According to the literature [31], paper fibers or ears of broadleaf cattails were used in white clay for wall paintings. The inclusion of *nori* in white clay remains uncertain; however, previous research [36] revealed that rice paste and hide glue were used for temple walls in the eighth century



- Chemical composition of clay is similar to Amakusa pottery clay [23]
- Paper fiber was used as *susa* [19]
- Rice paste or animal glue was used as a material for walls in 700s in Japan, although it has been unclear the white clay contains *nori* [22]

Fig. 2 Assumption of the material composition of the *Hiten* wall paintings

Table 1 Mass compositions of white clay used in Horyu-ji Temple and Amakusa pottery clay (%)

	SiO ₂	Al ₂ O ₃	Fe ₂ O ₃	CaO	MgO	Alkali	Ignition loss
Fragment of wall paintings at the main hall in Horyu-ji Temple (averaged value)	78.79	11.36	2.52	0.99	0.15	5.17	0.73
Amakusa pottery clay	78.03	14.50	0.68	0.06	0.13	–	4.61

in Japan. It is important to note that the assumptions made regarding the material composition of the wall paintings in this research do not definitively determine the material composition of the wall paintings in the main hall of Horyu-ji Temple. Further comprehensive literature reviews and scientific investigations are necessary to clarify the precise material compositions of wall paintings.

Materials

Although the assumption of materials in the white clay of the *Hiten* wall paintings is shown above, the precise mixing ratio of the materials remains unclear. In this study, samples with different material mixing ratios were prepared to obtain data within a certain range, and the dependence of the mechanical properties on the material mixing ratio was analyzed in addition to the humidity dependence. The materials used for the samples are as follows. Commercially available Amakusa pottery clay, commonly used in ceramic art, was used. Table 1 compares the results of the compositional analysis of the burned wall painting fragments [35] with the composition of the Amakusa pottery clay used in this study. In the existing literature, chemical analysis was performed on burnt fragments of white clay from the 12 large wall paintings. The values in Table 1 are the average of the results. The chemical composition of Amakusa pottery clay is based on compositional information of the product. Paper fiber was used as *susa*. Paper fiber is also commercially available as a plastering material. In traditional plastering work, paper fibers are soaked in water before being added to the clay paste. In this study, the paper fiber was soaked for at least 12 h before being mixed with the clay. Rice glue was used as *nori*. Commercially available rice flour is dissolved in water and heated to produce rice glue. After cooling to room temperature, the rice content was controlled by adjusting the water content while the weight was measured. Ten percent rice glue (10 g of rice glue contain 1 g of rice flour) was used to prepare the specimens. Distilled water was used to fabricate the specimens, including the water used for soaking the paper fibers and making the rice glue.

In plaster work today, paper fiber is typically added amounting to approximately 1% of the mass of the soil. In this study, compositions were examined with 0%, 1%,

and 3% of paper fibers relative to the mass of clay, including compositions with a relatively higher amount of paper fiber. On the other hand, rice glue is not commonly used in plaster work today. If rice glue was mixed in, the ratio to clay was small because adding a large amount of rice glue could increase the risk of damage by fungi and worms. However, our specimens without rice glue were weak and cracked in areas where strain gauges were attached due to the drying shrinkage of adhesive for the gauges. As a result of preliminary studies, we determined that the minimum mixing ratio of rice flour required for attaching strain gauges was 0.5% to the mass of clay. Compositions were examined with 0.5%, 1%, and 2% rice flour, including compositions with increased mixing ratios. Collectively, nine material-mixing patterns were examined, with a combination of three patterns for paper fiber and rice glue. Table 2 lists the material compositions of each pattern. Amakusa pottery clay, paper fiber, and rice flour masses were measured at equilibrium at 53% RH. The mass of water included the water in the soaked paper fiber, in addition to the water directly added. The water mass was adjusted by mixing all the other materials and adding water to achieve the desired total mass.

Table 2 Quantities of materials in simulated white clay

Sample species	Amakusa pottery clay (g)	Paper fiber (g)	Rice glue (g) containing 10% rice flour	Water (g)
P0R05	100	0	5	27.5
P0R1	100	0	10	23
P0R2	100	0	20	14
P1R05	100	1	5	31.5
P1R1	100	1	10	27
P1R2	100	1	20	18
P3R05	100	3	5	39.5
P3R1	100	3	10	35
P3R2	100	3	20	26

The names for the sample species use the letters "P" and "R" to represent paper fiber and rice flour, respectively. The numerical values indicate the corresponding mixing ratios. For instance, P1R05 means a mixture of 1% paper fiber and 0.5% rice flour relative to the mass of clay. The use of a single "P" or "R" refers to all three patterns of material mixing ratios that include paper fiber or rice flour in the following test. For example, P1 refers to the mixing ratios P1R05, P1R1, and P1R2

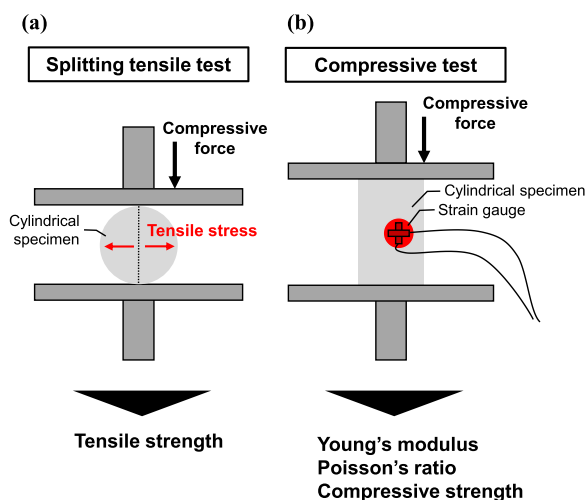


Fig. 3 Diagrams of the tensile splitting test and compressive test

Methods

Principle of the tests

In the splitting tensile test (also called the Brazilian test), the cylindrical specimen is placed so that the sides of the specimen are subjected to compressive test force (Fig. 3a). The maximum tensile stress occurred in the center surface (dotted line in Fig. 3a) in the direction perpendicular to the test force, and the specimen broke by the tensile force. When the base shape remained circular, tensile strength σ_{ten} (MPa) was determined using the following equation:

$$\sigma_{ten} = \frac{2P_t}{\pi D_0 L_0}, \quad (1)$$

where D_0 (m) is the diameter of the specimen, L_0 (m) is the height of the specimen, and P_t (MN) is the test force at failure [37]. The damage criteria based on strain, such as strain at failure or yield strain, is usually used to predict damage to cultural properties, mainly because the stress can relax over time. However, in the splitting tensile test, the directions of the test force and tensile force that breaks the specimen are different. Furthermore, the tensile stress and corresponding strain are varied in the direction perpendicular to the direction of the test force. These made obtaining critical strain using a testing machine or strain gauge challenging. Thus, obtaining damage criteria based on strain is a problem to be addressed in future studies.

The compressive test involved applying an axial compressive force to an unconstrained cylindrical specimen (Fig. 3b). The testing machine recorded the displacement corresponding to the test force, and the stress–strain relationship was calculated using the previously measured dimensions of the specimen. The compressive strength

was obtained from the stress at fracture, whereas Young's modulus was determined from the initial slope. The axial and circumferential strains were measured using an orthogonal strain gauge attached to the side of the specimen. Poisson's ratio was calculated based on the relationship between the two strains.

In both tests, the results must be considered in light of the conservation of cultural artifacts, and any irreversible deformation or cracking is considered damage. We obtained the strength from the test force when the clay part of the specimen cracked even though the specimen was still able to withstand the test force.

Preparation of samples

Commercially available metal water-pipe parts were utilized as molds for the test specimens. For the splitting tensile test, molds with a nominal diameter of 32 mm and a length of 50 mm were employed. For the compressive test, molds with a nominal diameter of 32 mm and a length of 75 mm were used. The inner surface of the mold was wrapped with a polychloroprene rubber sheet to protect the specimens from damage during drying shrinkage. The molds were positioned on a sponge sheet and filled with a mixed clay paste. The specimens were allowed to dry naturally in a laboratory room from August to November (summer to autumn in Japan) without temperature or humidity control. After 1 week, the molds were removed, and the specimens were left to dry for another two weeks. The top and bottom surfaces of the specimens were sanded with #80 sandpaper to obtain smooth surfaces. The height of the specimens used in the splitting tensile test was approximately 35 mm, whereas that used in the compressive test was approximately 55 mm. Both specimens had a diameter of approximately 30 mm. Following the hardening of the specimens, their dimensions were measured using digital calipers and they were placed in desiccators containing a saturated salt solution to achieve specific equilibrium humidity levels. We selected four equilibrium humidity levels: 33% RH, 53% RH, and 84% RH in addition to oven dry (105 °C) regarded as 0% RH. The tests were conducted at least 14 days after the initiation of oven drying and after at least 90 days for specimens at the other humidity levels. We used five specimens per material mixing ratio and equilibrium humidity level for the splitting tensile tests. Three specimens were used for the compressive tests.

Measurement system and testing methods

The measurement system used in the experiments is shown in Fig. 4. A compact table-top universal testing machine (EZ-LX, Shimadzu Co.) with a load cell capacity of 5 kN was employed. The splitting tensile and compressive tests were conducted within a thermostatic chamber

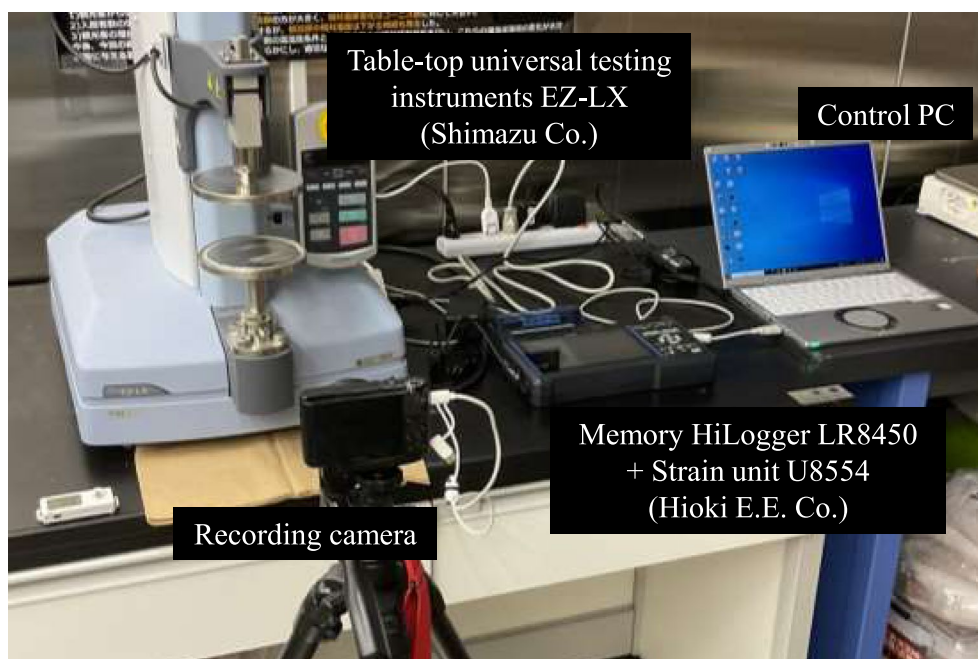


Fig. 4 Measuring system for splitting tensile and compressive tests

at a temperature of 23 °C. Humidity was not actively controlled, and the humidity levels ranged from 14 to 30% RH during the splitting tensile test and 19–26% RH during the compressive test. Before testing, the oven-dried specimens were placed in a desiccator containing a desiccant agent (silica gel) in the thermostatic chamber for approximately one hour to cool. In the compressive test, strain gauges were attached to specimens at equilibrium humidities of 33%, 53%, and 84% RH for measuring Poisson's ratio. The test was conducted after the adhesive was allowed to dry for at least 48 h. We used strain gauges KFGS-10-120-D16-11 and adhesive CC-36 (Kyowa Electronic Instruments Co., Ltd.). The strain was recorded using a HiLogger LR 8450 memory connected to a strain measuring unit U8554 (both manufactured by Hioki E. E. Co.).

The loading rate was controlled in both tests. For the splitting tensile test, it was determined based on the "Method for splitting tension test on rocks" (JGS 2551-2020) [37]. According to this standard, the loading rate should be set such that the failure time is between 1 and 15 minutes. We selected a loading rate of 0.1 mm/min and ceased loading when cracks were observed at the base of the specimens, which typically occurred more than 10 min from the start of loading. Due to an error, the tests for the specimens P0R05 at oven-dried, 53%, and 84% RH; P0R1 at 53% and 84% RH; P0R2 at 53%

RH; and P1R05 at oven-dried were conducted at a loading rate of 1 mm/min. To investigate the effect of loading rate, we conducted additional tests at a loading rate of 1 mm/min for each specimen of P1R2 and P3R1 at oven-dried, which were spare specimens. The tensile strength for these specimens was approximately 0.81 times and 1.29 times that of the specimens tested at 0.1 mm/min, respectively. The coefficient of variation was less than 0.26 for all combinations of examined equilibrium humidities and material mixing ratios at a loading rate of 0.1 mm/min. The 1 mm/min test results are not expected to deviate significantly from the range of the 0.1 mm/min test results. Therefore, we considered that the effect of the loading rate was not so significant, and we combined the results for both loading rates. Ideally, additional tests and a statistical basis would be needed to determine how to treat the test results. However, the small number of test specimens available for this study made a detailed comparison difficult. In the compressive test, the loading rate was determined based on the "Method for unconfined compression test on rocks" (JGS 2521-2020) [37]. According to this standard, the specimens are to be subjected to displacement at a rate of 0.01–0.1% strain per minute. Therefore, we set the loading rate to 0.05 mm/min for the test and stopped the loading once the displacement exceeded 1 mm. Cracks on the sides of the specimens were confirmed visually.

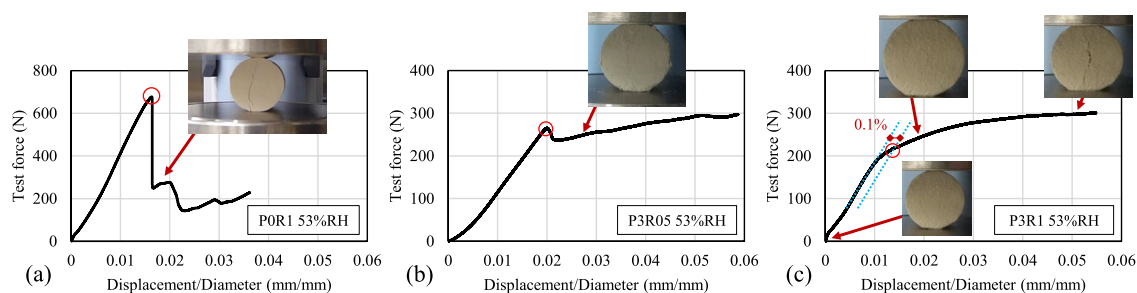


Fig. 5 Typical test force–displacement/diameter relationships in splitting tensile test. **a** specimens without paper fiber, **b** and **c** those with paper fiber

Results

Tensile strength

Due to the differences in the fracturing behavior based on the presence or absence of paper fibers in the specimens, we modified the methods for determining the maximum test force. These methods are described below, along with the corresponding figures. Figure 5a illustrates a typical test force–displacement/diameter relationship for specimens without paper fibers (P0). Initially, the test force increased linearly with displacement/diameter, followed by a sudden decrease. Cracking on the base surface was observed immediately after the decrease in the test force. In this case, the specimens were considered to have undergone brittle fracture. To calculate the tensile strength, we used the maximum test force recorded throughout the dataset (indicated by the red circle in Fig. 5a). Conversely, Fig. 5b, c depict typical test force–displacement/diameter relationships for specimens containing paper fiber (P1 and P3). As shown in Fig. 5b, the test force increased linearly with increasing displacement/diameter, temporarily decreased, and then increased again. The cracking of the base occurred after the initial decrease in the test force. As shown in Fig. 5c, as the test force continued to increase, the slope decreased. Cracking was observed when the slope decreased. The tensile strength was calculated differently, depending on the case. For the former case, we determined the tensile strength from the test force immediately before the initial decrease (red circle in Fig. 5b). For the latter scenario, we derived the tensile strength from the test force at which the displacement/diameter exceeded 0.1% of the initial slope line (red circle in Fig. 5c). It is important to note that the reference standards for the splitting tensile test assumed brittle fracture, whereas the methods used to determine the test force for calculating the tensile strength were established so that the results could be used for predicting damage to cultural artifacts.

In our study, we removed outliers for combinations of humidity and mixing ratios where the coefficient of variation exceeded 0.30. We considered 159 values out of a

total of 180 test results (3–5 specimens for each of the 36 combinations) valid. The coefficient of variation was less than 0.26 for all the combinations. Figure 6 illustrates the measured and mean tensile strengths for each material mixing ratio regarding the equilibrium relative humidity (RH). Each plot presents the results of three material mixing ratios containing the same paper fiber or rice flour. The left column shows P0, P1, and P3 from top to bottom, whereas the right column shows R05, R1, and R2. The small dots represent individual measurements, whereas the large dots indicate mean values. The dotted lines represent plots of the approximated functions, the details of which are provided in the analysis section of the Discussion. (Figs. 8 and 9 follow the same plot style). The mean tensile strength ranged from 0.0785 to 1.17(MPa) for all the material mixing ratios, with significant variations depending on the equilibrium RH and material mixing ratio. As the humidity increases, the strength decreases. Specifically, the tensile strength at 84% RH was only 21–37% of that measured for oven-dried specimens. Moreover, the higher the humidity, the smaller the difference in tensile strength between the different material mixing ratios. When examining the material mixing ratio, we observed that the strength was higher at 2% rice flour for the same mixing ratio of paper fibers. Furthermore, the strength tends to be higher with a lower mixing ratio of paper fibers when comparing the same mixing ratio of rice flour.

Compressive strength

Figure 7a–c present typical examples of the stress–strain relationships observed in the compressive test. In most specimens, as depicted in Fig. 7a, b, the stress deviated from a linear relationship and reached a maximum value regardless of the paper fiber mixing ratio. In some specimens, as illustrated in Fig. 7a, side cracking occurred before reaching the maximum stress. For specimens with 3% paper fiber, as Fig. 7c shows, cracking occurred after the slope of the stress–strain relationship decreased, and

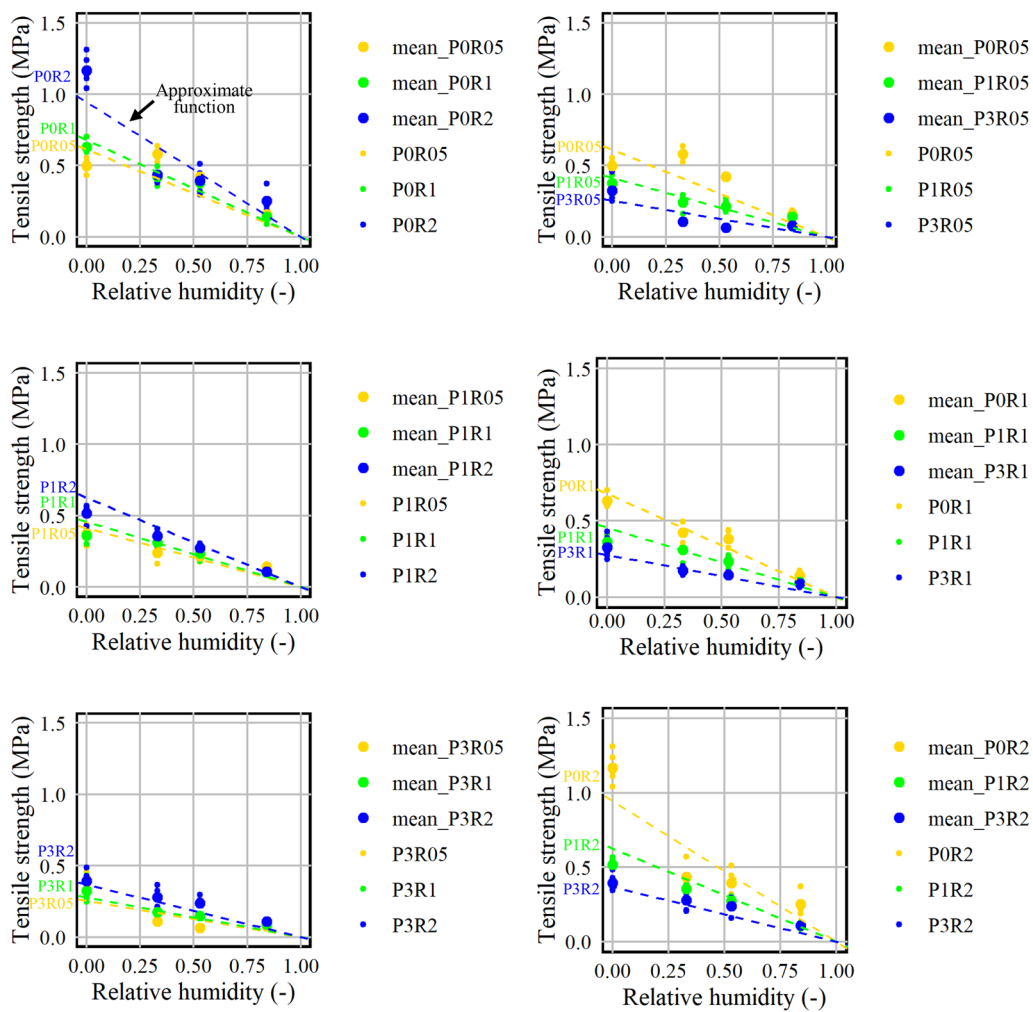


Fig. 6 Tensile strength for each material mixing ratios concerning equilibrium RH

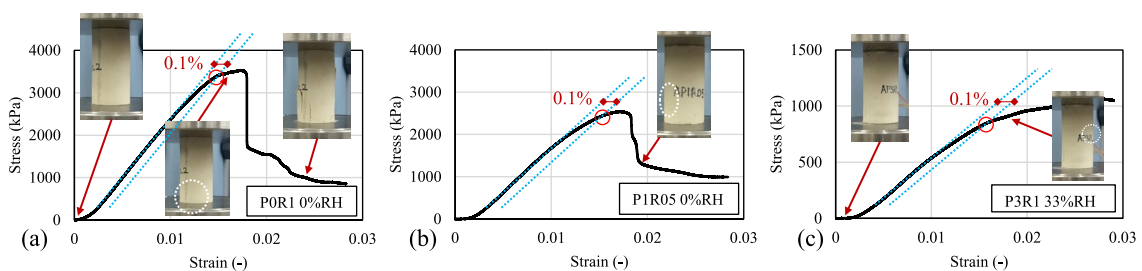


Fig. 7 Typical stress–strain relationships in a compressive test. **a** specimens without paper fiber, **b** and **c** those with paper fiber

the stress continued to increase after that. In all cases, we calculated the compressive strength from the test force at which the strain deviated by 0.1% from the initial slope line (red circles in Fig. 7).

We considered all three measured specimens for each combination of humidity and material mixing ratio as valid for measuring the compressive strength. The

compressive strengths obtained from these measurements, along with the corresponding mean values for each material mixing ratio, are shown in Fig. 8. The mean compressive strength ranged from 0.358 to 3.67 (MPa) and generally exhibited a decrease with increasing RH for all material mixing ratios. At an equilibrium RH of 84%, the compressive strength was approximately 32–63% of

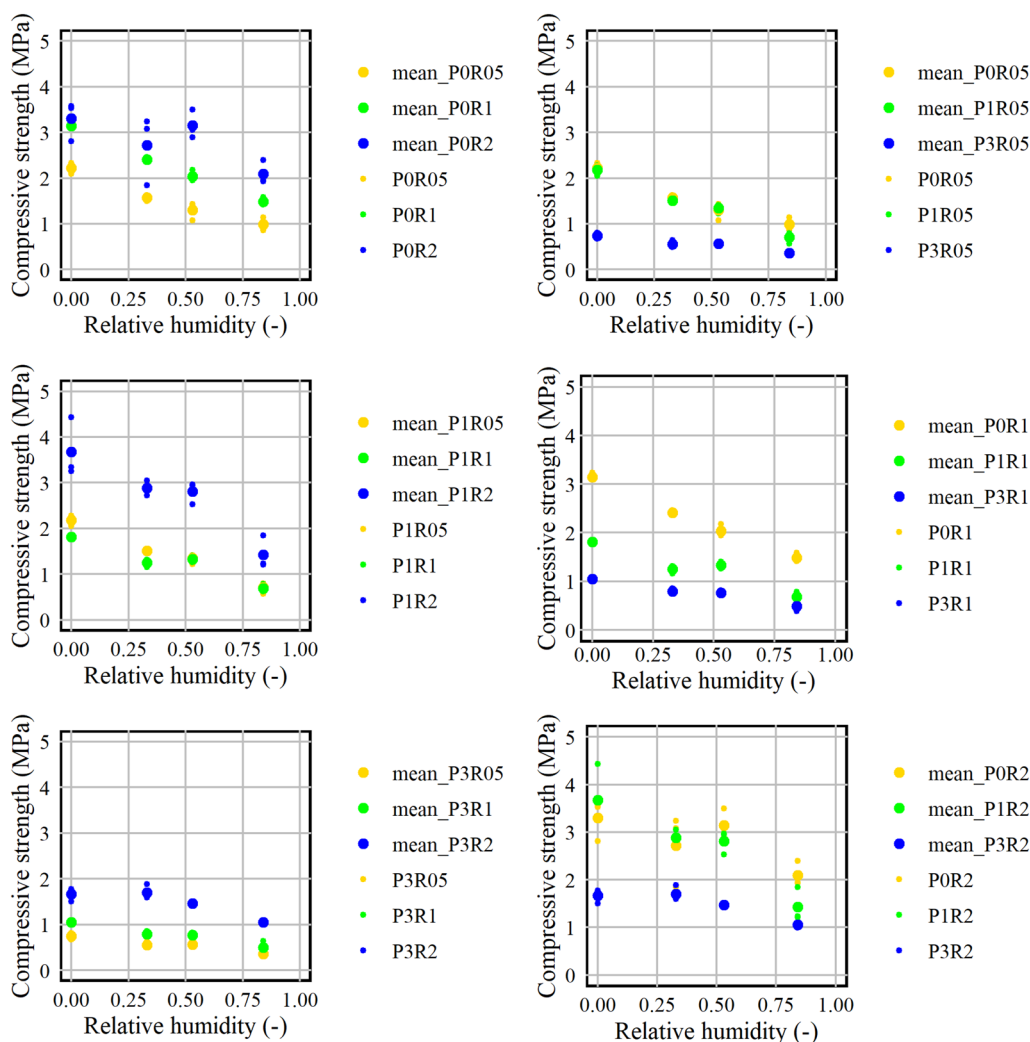


Fig. 8 Compressive strength for each material mixing ratios concerning equilibrium RH

that observed for oven-dried specimens. Regarding the material mixing ratio, the compressive strength tends to be higher with a higher mixing ratio of rice flour or a lower mixing ratio of paper fibers. When comparing the compressive strength and tensile strength at the same humidity and material mixing ratio, the tensile strength was only 10–43% of the compressive strength. This confirms that white clay is weaker in tension, which is consistent with the behavior of many earthen materials. Furthermore, when comparing the tensile strength at 33% equilibrium RH with the compressive strength at 84% RH for the same material mixing ratio, the tensile strength was 21–59% of the compressive strength. This implies that tensile fractures are more likely to occur than compressive fractures when the moisture content in white clay is distributed and the degree of deformation is distributed accordingly.

Young’s modulus and Poisson’s ratio

To determine Young’s modulus, we considered all three measured specimens for each combination of humidity and material mixing ratios as valid for identifying the compressive strength. Figure 9 illustrates the measured and mean Young’s moduli for each material mixing ratio regarding the equilibrium RH. The mean Young’s modulus ranged from 0.0394 to 0.274 (GPa) and exhibited variations depending on the humidity and material mixing ratio. Young’s modulus generally decreased as humidity increased for all material mixing ratios. The magnitude of this decrease was substantial from 53% RH to 84% RH, with the value at 84% equilibrium RH representing approximately 45–69% of that at 53% equilibrium RH. Regarding the material mixing ratio, Young’s modulus tends to increase with a decreasing mixing ratio of paper fiber or an increasing mixing ratio of rice flour.

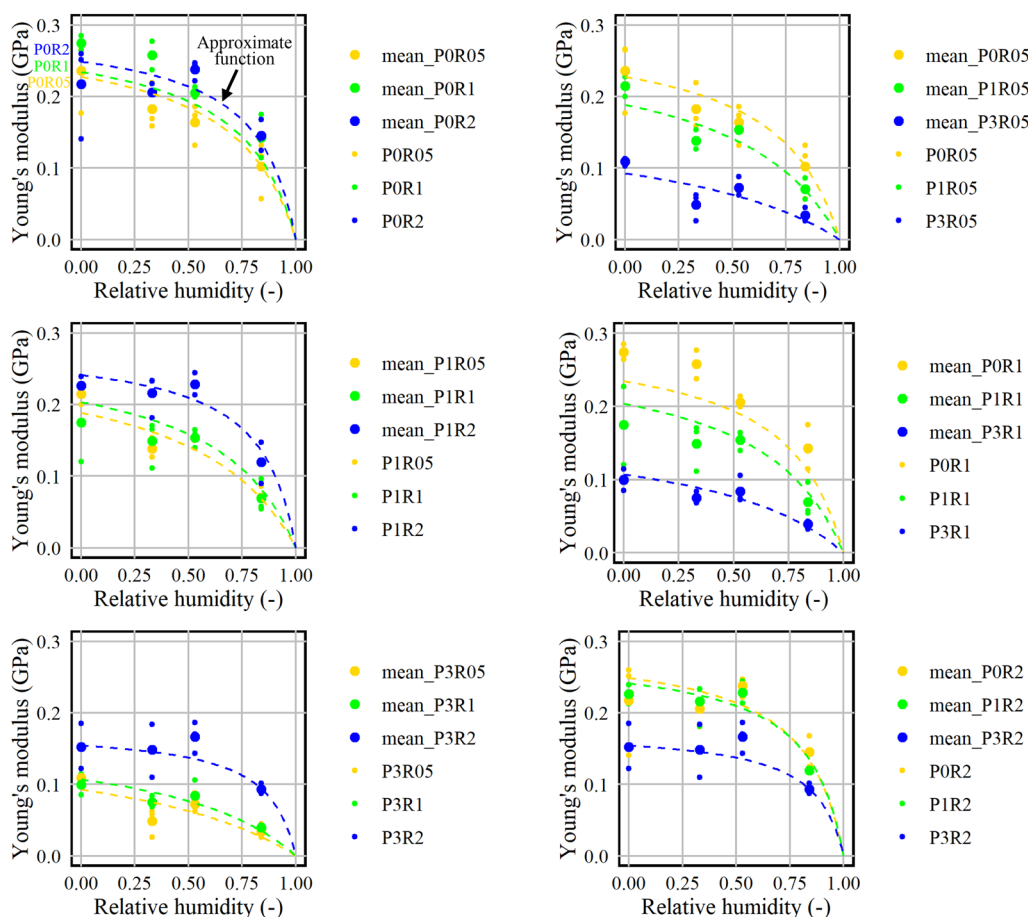


Fig. 9 Young's modulus for each material mixing ratios concerning equilibrium RH

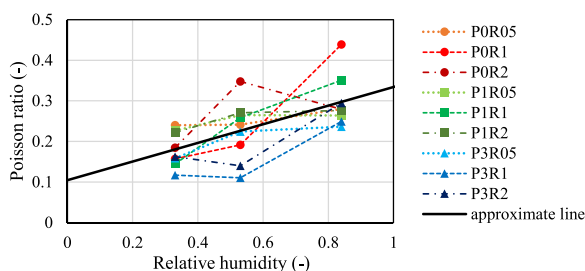


Fig. 10 Mean Poisson's ratio for each material mixing ratio concerning equilibrium RH

For measuring the Poisson's ratio, we considered one to three results valid for each humidity and material mixing ratio. The strain gauges attached to the white clay specimens came off easily, which made the measurement difficult. We considered available 98 results out of a total of 108 measurements as valid. Figure 10 illustrates the mean Poisson's ratio for each material

mixing ratio regarding equilibrium RH. The values ranged from 0.11 to 0.44 (-). Poisson's ratio tends to increase as the humidity increases, with the value at 84% equilibrium RH being larger than that at 33% RH. On the other hand, the effect of the material mixing ratio on Poisson's ratio was not discernible.

Discussions

Effect of humidity and material mixing ratio on mechanical properties of white clay

The tensile strength, compressive strength, and Young's modulus of white clay tend to decrease as equilibrium RH increases. It is considered that the macroscopic strength and elasticity of white clay are governed by the bonds between the clay particles. Further, the bond intensity is influenced by the attraction of the meniscus formed among the particles. This attraction depends on factors such as the capillary pressure, surface tension of the liquid water, and meniscus shape [38]. The capillary pressure decreases as equilibrium humidity increases, which may reduce the intensity of the bond between the clay

particles, leading to a decrease in both the strength and in Young’s modulus. Conversely, Poisson’s ratio of white clay increased as equilibrium RH increased. Previous studies have also shown that Poisson’s ratio of unsaturated soils increases as the degree of saturation increases [39, 40]. In porous materials, the Poisson’s ratio is close to zero when compression causes pore collapse, thereby reducing the volume. It reaches 0.5 when there is no volumetric change. As equilibrium humidity increases, the elasticity of the solid part in the white clay decreases, whereas the pore pressure increases, which may make the pores relatively less collapsible. This can result in an increased Poisson’s ratio at higher humidity levels.

Young’s modulus and the compressive strength of the white clay with a relatively higher mixing ratio of paper fibers demonstrated a decreasing trend. The tensile strength also decreased although the test force was supported after the clay cracked. The physical properties of earthen materials mixed with fibrous materials have been studied in geotechnical engineering and building materials research such about soil blocks [41–47]. A simple comparison of the properties is difficult because research focusing on structural strength typically considers fractures as a loss of support. Nevertheless, the compressive or tensile strengths of such materials vary according to the type of added material, mix ratio, and density determined by compression during sample preparation [41–46]. In studies that measured the shear properties of soil mixed with jute fiber [47] and the tensile strength of compacted soil mixed with polypropylene fiber [46], it was discussed that the binding between soil particles and fiber is a crucial factor for achieving shear and tensile strength, respectively. Concerning white clay, which was dried without compaction, it is likely that an increased mixing ratio of paper fibers reduces the contact area between the clay particles. This could weaken their bonds, resulting in diminished macroscopic mechanical properties. In contrast, the tensile strength, compressive strength, and Young’s modulus of white clay with a high mixing ratio of rice flour exhibited an increasing trend, indicating that rice glue potentially intensified the bonds between the clay particles. However, regardless of the mixing ratio of rice flour, a decreasing trend in the mechanical properties with increasing humidity remained observable, indicating that the primary bonding mechanism in white clay could be a meniscus attraction.

Regarding the change in mechanical properties due to rice glue mixing, studies on historical building materials in China have presented an increase in the compressive strength of the mortar [48]. The literature attributes this to the chemical action during lime hardening, which hardens the pore structure. This mechanism cannot

be applied to white clay, in which the clay particles are bonded by the meniscus.

A more detailed elucidation of the effect of the material mixing ratio on the mechanical properties would necessitate microstructural observations, such as scanning electron microscopy or X-ray computed tomography. Furthermore, evaluating the difference in fracture behavior with changes in the material mixing ratio through splitting tensile and compressive tests is challenging. Therefore, tests for fracture toughness and other parameters must be included in future measurements.

Analysis of obtained data

We present the measured mechanical properties as functions of the equilibrium RH and material mixing ratio so they can be used in predicting deformation and damage to wall paintings. A numerical model of tensile strength is presented given that tensile fracture precedes compressive fracture in white clay. The relationship between tensile strength σ_{ten} (MPa) and equilibrium RH $h(-)$ can be represented as a proportionality equation, where the tensile strength becomes zero at an RH of 1:

$$\sigma_{ten} = \alpha(1 - h), \tag{2}$$

where coefficient α was determined using the least-squares method for each material mixing ratio. As the paper fiber mixing ratio $p(\%)$ increased, the coefficient α decreased monotonically, following a downward convex curve. The coefficient displays a similar curve and monotonically increases as the mixing ratio of rice flour $r(\%)$ increases. We express the coefficient α as a function of the extremum values at $p = 3$ and $r = 0$:

$$\alpha = a_1 - 6a_2p + a_2p^2 + a_3r^2 - 6a_4pr^2 + a_4p^2r^2, \tag{3}$$

where the values of coefficients $a_1 \sim a_4$ were obtained using the least-squares method and are listed in Table 3. The coefficient of determination for this approximate function was 0.85. The functional lines are indicated by dotted lines in Fig. 6. As this approximate function is

Table 3 Coefficients of Eq. (3)

Coefficient	Value
a_1	0.5899
a_2	3.818×10^{-2}
a_3	8.875×10^{-2}
a_4	6.466×10^{-3}

based on the measurements, the valid range is $0 < p < 3$ and $0.5 < r < 2$. (The valid ranges for Eqs. (5) and (6) also correspond to this).

Moreover, we present the coefficients of the elastic constitutive law, Young’s modulus E (GPa), and Poisson’s ratio $\nu(-)$, as approximate functions. We express Young’s modulus as a function that decreased as equilibrium RH increased, and the decrease became more significant at high humidity levels, reaching zero when the RH was 1.

$$E = \frac{\beta_1(1 - h)}{1 - h + \beta_2}, \tag{4}$$

where the coefficients β_1 and β_2 were determined using the least-squares method for each material mixing ratio. The coefficient β_1 tends to decline as the mixing ratio of the paper fiber increases. We represent the relationship as a function of only the mixing ratio of paper fiber, irrespective of the mixing ratio of rice flour:

$$\beta_1 = b_1 + b_2p^2. \tag{5}$$

We expressed coefficient β_2 as a function that varies linearly with the mixing ratio of paper fiber and rice flour:

$$\beta_2 = c_1 + c_2p + c_3r + c_4pr, \tag{6}$$

where the coefficients $b_1, b_2, c_1 \sim c_4$ were determined using the least-squares method and are listed in Tables 4 and 5. The coefficient of determination in Eq. (4) is 0.90, and the function is represented by the dotted curves in Fig. 9. As for the Poisson’s ratio, no dependency on the material mixing ratio was observed; therefore, we expressed it as a linear function with consistent coefficients regarding the equilibrium RH:

$$\nu = \gamma_1h + \gamma_2, \tag{7}$$

where the coefficients γ_1 and γ_2 were determined using the least-square method and are displayed in Table 6. The coefficient of determination was 0.42. Although the approximation lacks sufficient accuracy, it illustrates a correlation between Poisson’s ratio and humidity. An approximate line is shown in Fig. 10.

Table 4 Coefficients of Eq. (5)

Coefficient	Value
b_1	0.2969
b_2	-1.346×10^{-2}

Table 5 Coefficients of Eq. (6)

Coefficient	Value
c_1	0.3410
c_2	0.2704
c_3	-7.377×10^{-2}
c_4	-0.1441

Conclusions

White clay was used in Japan from the 7th to the fourteenth century to construct substrates for wall paintings and Buddhist statues, including in existing cultural artifacts designated as important cultural properties or national treasures of Japan. However, the mechanical properties of white clay remain unknown. In this study, we aimed to obtain the strength and elastic coefficients of white clay by simulating the substrate of *Hiten* wall paintings in the main hall of the Horyu-ji Temple towards constructing a deformation and damage prediction model.

We performed splitting tensile tests to obtain the tensile strength and compressive tests to determine the compressive strength, Young’s modulus, and Poisson’s ratio. The specimens were prepared at different equilibrium humidities (from oven-dried to 84% RH) and various material mixing ratios (0–3% of paper fiber and 0.5–2% of rice flour to the mass of clay), and their effects on the mechanical properties were evaluated. The tests revealed that the tensile strength, compressive strength, and Young’s modulus ranged from 0.0785–1.17(MPa), 0.358–3.67(MPa), and 0.0394–0.274 (GPa), respectively, with the variations dependent on the equilibrium humidity and material mixing ratio. The tensile strength, compressive strength, and Young’s modulus decreased as equilibrium RH increased. These properties also tended to decrease with a higher mixing ratio of paper fibers or a lower mixing ratio of rice flour. Notably, the tensile strength was lower than the compressive strength at the same humidity and material mixing ratio, suggesting a greater likelihood of tension-induced fractures in white clay. Furthermore, the tensile strength at 33% equilibrium RH is lower than the compressive strength at 84% equilibrium RH for the same material mixing ratio. This indicates that tensile fracture is more likely to occur first

Table 6 Coefficients of Eq. (7)

Coefficient	Value
γ_1	0.2297
γ_2	0.1043

when white clay deforms, owing to the moisture content distribution.

We also represented the tensile strength and Young's modulus as functions of the equilibrium humidity and material mixing ratio to be used in predicting deformation and damage to wall paintings. The mean Poisson's ratios for each humidity and material mixing ratio ranged from 0.11 to 0.44 (–). These values were typically higher at 84% equilibrium RH than at 33% RH, whereas the dependence on the material mixing ratio was not explicit. We provided an approximate line for Poisson's ratio regarding the equilibrium RH. Given that these macroscopic mechanical properties are likely influenced by the microscopic bonds of clay particles, further research, including microstructural observations, is essential to elucidate the effects of humidity and material mixing ratio on these mechanical properties in detail.

Our findings on white clay can be applied to the conservation and repair work of cultural artifacts made from white clay, including the target wall paintings. In future research, we aim to quantitatively clarify the relationship between the moisture state and deformation of white clay. We also plan to examine the mechanical properties of other materials in the lower layers of the target wall paintings and construct a comprehensive deformation and damage prediction model for these cultural artifacts.

Abbreviation

RH Relative humidity

Acknowledgements

The authors would like to thank persons of Horyu-ji temple, The Ashahi Shinbun Company and Agency for Cultural Affairs (Government of Japan) in office of the committee for the conservation and exhibition project of wall paintings at the main hall, *Kondo* in Horyu-ji Temple. The authors also gratefully acknowledge the opportunity to discuss the composition of the wall paintings with Dr. Norimasa Aoyagi, Associate Professor at Ritsumeikan University. Finally, we would like to thank English editing service Editage (www.editage.jp) for improving readability of this paper.

Author contributions

KI fabricated the samples, performed all measurements, analyzed data, and was a major contributor in writing the manuscript. DO, CI, NT, and SW helped fabricating samples, carrying out the measurements, and analyzing data and reviewed the manuscript. All authors read and approved the final manuscript.

Funding

Part of the present work was supported by the Grant-in-Aid for JSPS Fellows of Japan Society for the Promotion of Science (Grant Number 22J15027 and 22KJ1975) and by the JST SPRING of Japan Science and Technology Agency (Grant Number JPMJSP2110). These supports were greatly appreciated.

Availability of data and materials

All data needed to evaluate the conclusions are present in this paper. Additional datasets used and analyzed during the current study are available from the corresponding author upon reasonable request.

Declarations

Competing interests

The authors declare that they have no competing interests.

Author details

¹Department of Architecture and Architectural Engineering, Graduate School of Engineering, Kyoto University, C2-411, Kyoto Daigaku-Katsura, Kyoto Nishikyō-Ku, Kyoto 6158540, Japan. ²Conservation Science Section, Nara National Research Institute for Cultural Properties, National Institutes for Cultural Heritage, Nara Nijo-Cho 2-9-1, Nara, Japan.

Received: 24 July 2023 Accepted: 11 November 2023

Published online: 21 November 2023

References

- Harriman L, Brundrett G, Kittler R. Humidity control design guide for commercial and institutional buildings. Atlanta: American Society of Heating, Refrigerating and Air-Conditioning Engineers; 2001.
- Jakiela S, Bratasz Ł, Kozłowski R. Numerical modelling of moisture movement and related stress field in lime wood subjected to changing climate conditions. *Wood Sci Technol*. 2008;42:21–37.
- Soboń M, Bratasz Ł. A method for risk of fracture analysis in massive wooden cultural heritage objects due to dynamic environmental variations. *Eur J Wood Prod*. 2022;80:1201–13.
- Matsumoto M, Iwamae A. An analysis of temperature and moisture variations in the ground under natural climatic conditions. *Energy Build*. 1988;11:221–37.
- Mecklenburg MF, Tumosa CS. Mechanical behavior of paintings subjected to changes in temperature and relative humidity. In: Mecklenburg MF, editor. *Art in transit: studies in the transport of paintings*. Washington, DC: National Gallery of Art; 1991. p. 173–216.
- Mecklenburg MF, Tumosa CS, Erhardt D. Structural response of painted wood surfaces to changes in ambient relative humidity. In: Dorge V, Howlett FC, editor. *Painted wood: history and conservation*. Los Angeles, CA: The Getty Conservation Institute. 1998; p. 464–483.
- Mecklenburg MF. Determining the acceptable ranges of relative humidity and temperature in museums and galleries, part 1, structural response to relative humidity. 2007.
- Mecklenburg MF. Determining the acceptable ranges of relative humidity and temperature in museums and galleries, part 2, structural response to temperature. 2007.
- Mazzanti P, Togni M, Uzielli L. Drying shrinkage and mechanical properties of poplar wood (*Populus alba* L.) across the grain. *J Cult Herit*. 2012;13S:S85–9.
- Rachwał B, Bratasz Ł, Łukowski M, Kozłowski R. Response of wood supports in panel paintings subjected to changing climate conditions. *Strain*. 2012;48:366–74.
- Janas A, Fuster-López L, Andersen CK, Escuder AV, Kozłowski R, Poznańska K, Gajda A, Scharff M, Bratasz Ł. Mechanical properties and moisture-related dimensional change of canvas paintings—canvas and glue sizing. *Herit Sci*. 2022;10:160.
- Rachwał B, Bratasz Ł, Krzemień L, Łukowski M, Kozłowski R. Fatigue damage of the gesso layer in panel paintings subjected to changing climate conditions. *Strain*. 2012;48:474–81.
- Bratasz Ł, Akoglu KG, Kékicheff P. Fracture saturation in paintings makes them less vulnerable to environmental variations in museums. *Herit Sci*. 2020;8:11.
- Janas A, Mecklenburg MF, Fuster-López L, Kozłowski R, Kékicheff P, Favier D, Andersen CK, Scharff M, Bratasz Ł. Shrinkage and mechanical properties of drying oil paints. *Herit Sci*. 2022;10:181.
- Bridarolli A, Freeman AA, Fujisawa N, Łukowski M. Mechanical properties of mammalian and fish glues over range of temperature and humidity. *J Cult Herit*. 2022;53:226–35.

16. Bridarolli A, Nualart-Torroja A, Chevalier A, Odlyha M, Bozec L. Systematic mechanical assessment of consolidants for canvas reinforcement under controlled environment. *Herit Sci.* 2020;8:52.
17. Luimes RA, Suiker ASJ. Numerical modelling of climate-induced fracture and deformation in wood: application to historical museum objects. *Int J Solids Struct.* 2021;210–211:237–54.
18. Bosco E, Suiker ASJ, Fleck NA. Crack channelling mechanisms in brittle coating systems under moisture or temperature gradients. *Int J Fract.* 2020;225:1–30.
19. Bosco E, Suiker ASJ, Fleck NA. Moisture-induced cracking in a flexural bilayer with application to historical paintings. *Theor Appl Fract Mech.* 2021;112: 102779.
20. Zhang R, Wood JD, Young CRT, Taylor AC, Balint DS, Charalambides MN. A numerical investigation of interfacial and channelling crack growth rates under low-cycle fatigue in bi-layer materials relevant to cultural heritage. *J Cult Herit.* 2021;49:70–8.
21. Zhang R, Taylor AC, Charalambides MN, Balint DS, Young CRT, Barbera D, Blades N. A numerical model for predicting the time for crack initiation in wood panel paintings under low-cycle environmentally induced fatigue. *J Cult Herit.* 2023;61:23–31.
22. Luimes RA, Suiker ASJ, Verhoosel CV, Jorissen AJM, Schellen HL. Fracture behaviour of historic and new oak wood. *Wood Sci Technol.* 2018;52:1243–69.
23. Schellmann NC. Delamination and flaking of East Asian export lacquer coatings on wood substrates. *East Asian Lacquer Material Culture, Science and Conservation.* In: Rivers S, Faulkner R, Pretzel B, editor. In association with the Victoria and Albert Museum, London. Published with the assistance of The Getty Foundation. Archetype Publications Ltd.; 2011.
24. Schellmann NC, Taylor AC. Establishing the fracture properties of delaminating multilayered decorative coatings on wood and their changes after consolidation with polymer formulations. *J Mater Sci.* 2015;50:2666–81.
25. Bratasz Ł, Łukowski M, Klisińska-Kopacz A, Zawadzki W, Dzierżęga K, Bartosik M, Sobczyk J, Lennard FJ, Kozłowski R. Risk of climate-induced damage in historic textiles. *Strain.* 2015;51:78–88.
26. Wilk D, Bratasz Ł, Kozłowski R. Shrinkage cracking in Roman cement pastes and mortars. *Cem Concr Res.* 2013;53:168–75.
27. Yamasaki K, Emoto Y. Pigments used on Japanese paintings from the protohistoric period through the 17th century. *Ars Orient.* 1979;11:1–14.
28. Hu K, Bai C, Ma L, Bai K, Liu D, Fan B. A study on the painting techniques and materials of the murals in the Five Northern Provinces' Assembly Hall, Ziyang. *China Herit Sci.* 2013;1:18.
29. Kaew-on N, Katemake P, Prasongsuk S. Primer formulations with antibacterial properties for murals. *Prog Org Coat.* 2020;138: 105395.
30. Mazzeo R, Baraldi P, Luján R, Fagnano C. Characterization of mural painting pigments from the Thubchen Lhakhang temple in Lo Manthang, Nepal. *J Raman Spectrosc.* 2004;35:678–85.
31. Fujii K. Integration of the report on the repair work for buildings of national treasures and important cultural properties (4th supplementation). Report on the repair work for conservation of national treasures in Horyu-ji Temple vol. 14. Tokyo: Bunsei Shoin; 1956 (in Japanese).
32. Introduction of Great Treasure Gallery in Horyu-ji Temple in home page of Horyu-ji Temple: <http://www.horyuji.or.jp/en/garan/daihozoin/>. Accessed on 28 Sept 2023.
33. Committee to investigate methods of conservating the wall paintings of Horyu-ji temple. Report on a survey of conservation methods for wall paintings of Horyu-ji Temple; 1920 (in Japanese) Available online: <https://dl.ndl.go.jp/pid/957032/1/1>. Accessed 31 Mar 2023.
34. Yamada S. Report on ancient wall paintings. Self-published; 1975 (in Japanese).
35. Shibata Y, Yamasaki K, Iwasaki T. Observation of drying condition after fire and chemical composition of wall paintings at Kondo in Horyu-ji temple. *Proc Jpn Acad.* 1950;8:207–11.
36. Yamada K. Literature review about plaster work in Nara period. *Transac Archt Inst Jpn.* 1960;65:129–34 (in Japanese).
37. Japanese geotechnical society. Japanese standards and explanations of laboratory tests of geomaterials (the first revised edition). Tokyo: Maruzen; 2020.
38. Butt H, Graf K, Kappl M. Physics and chemistry of interfaces. third, revised and enlarged edition. New York: Wiley; 2013.
39. Inci G, Yesiller N, Kagawa T. Experimental investigation of dynamic response of compacted clayey soils. *Geotech Test J.* 2003;26:125–41.
40. Thota SK, Cao TD, Vahedifard F. Poisson's ratio characteristic curve of unsaturated soils. *J Geotech Geoenviron Eng.* 2020. [https://doi.org/10.1061/\(ASCE\)GT.1943-5606.0002424](https://doi.org/10.1061/(ASCE)GT.1943-5606.0002424).
41. Oskoueï AV, Afzali M, Madadipour M. Experimental investigation on mud bricks reinforced with natural additives under compressive and tensile tests. *Constr Build Mater.* 2017;142:137–47.
42. Mazhoud B, Collet F, Pretot S, Lanos C. Mechanical properties of hemp-clay and hemp stabilized clay composites. *Constr Build Mater.* 2017;155:1126–37.
43. Boucheffa I, Bichri EL, Chehouani H, Benhamou B. Mechanical and thermophysical properties of compressed earth brick reinforced by raw and treated doum fibers. *Constr Build Mater.* 2022;318:126031.
44. Eslami A, Mohammadi H, Banadaki HM. Palm fiber as a natural reinforcement for improving the properties of traditional adobe bricks. *Constr Build Mater.* 2022;325: 126808.
45. de Castrillo MC, Ioannou I, Philokyrou M. Reproduction of traditional adobes using varying percentage contents of straw and sawdust. *Constr Build Mater.* 2021;294: 123516.
46. Li J, Tang C, Wang D, Pei X, Shi B. Effect of discrete fibre reinforcement on soil tensile strength. *J Rock Mech Geotech Eng.* 2014;6:133–7.
47. Yixian W, Panpan G, Shengbiao S, Haiping Y, Binxiang Y. Study on strength influence mechanism of fiber-reinforced expansive soil using jute. *Geotech Geol Eng.* 2016;34:1079–88.
48. Yang R, Zhang Z, Xie M, Li K. Microstructural insights into the lime mortars mixed with sticky rice sol-gel or water: a comparative study. *Constr Build Mater.* 2016;125:974–80.

Publisher's Note

Springer Nature remains neutral with regard to jurisdictional claims in published maps and institutional affiliations.

Daisuke Ogura DO belong to the committee for the conservation of the Kondo Murals at Horyu-ji. DO is the working group chair focusing on storage conditions, which studies the environment to preserve the wall paintings.

Soichiro Wakiya SW belong to the committee for the conservation of the Kondo Murals at Horyu-ji. DO is the working group chair focusing on storage conditions, which studies the environment to preserve the wall paintings.

Submit your manuscript to a SpringerOpen® journal and benefit from:

- Convenient online submission
- Rigorous peer review
- Open access: articles freely available online
- High visibility within the field
- Retaining the copyright to your article

Submit your next manuscript at ► [springeropen.com](https://www.springeropen.com)